# Direct electrodeposition of imidazole modified poly(pyrrole copolymers: synthesis, characterization and supercapacitive properties

Franciele Wolfart[a], Bruna M. Hryniewicz[a], Luís F. Marchesi[a,b], Elisa S. Orth[c], Deepak P. Dubal [d,e], Pedro Gómez-Romero[d], Marcio Vidotti[a],*

[a] Grupo de Pesquisa em Macromoléculas e Interfaces, Departamento de Química, Universidade Federal do Paraná, CP 19032, 81531-980 Curitiba, PR, Brazil
[b] Universidade Tecnológica Federal do Paraná, Av. Monteiro Lobato s/n Km 04, CEP 84016-210, Ponta Grossa, PR, Brazil
[c] Grupo de Catálise e Cinética, Departamento de Química, Universidade Federal do Paraná, CP 19032, 81531-980 Curitiba, PR, Brazil
[d] Catalan Institute of Nanoscience and Nanotechnology (ICN2), CSIC and The Barcelona Institute of Science and Technology, Campus UAB, Bellaterra, 08193 Barcelona, Spain
[e] School of Chemical Engineering, The University of Adelaide, Adelaide, South Australia 5005, Australia

## ABSTRACT

In this manuscript we report the direct electrosynthesis of a new conducting copolymer based on the incorporation of imidazole molecules within the polypyrrole chain. Different proportions of the monomers were tested during the direct electropolymerization of the copolymer. The resulting materials were characterized by electrochemical and spectroscopic techniques (Raman and XPS) and a mechanism of polymerization is proposed. Our findings showed that imidazole acts as an inhibitor of the polymerization process, decreasing the overall number of actives sites for the polymerization on the electrode surface producing a polymeric morphology very different compared with pure polypyrrole, as observed by Scanning Electron Microscopy images and corroborated by Electrochemical Impedance Spectroscopy. This behavior significantly affects the supercapacitive performance of the resulting p(PyIMZ) modified electrodes where the specific capacitance of the material increased from 122 to 201 $Fg^{-1}$ (64%) at 10 mV $s^{-1}$. Furthermore, a unique pseudo-capacitive behavior described herein emphasizes the role of the imidazole as inductor of the morphology and co-monomer in the unique electrochemical signature of the material. The results suggest that the incorporation of IMZ increases the specific capacitance of PPy electrode by around 64%.

## 1. Introduction

Polypyrrole (PPy) is one of the most studied conducting polymers within different areas of development such as sensor and biosensors [1], artificial muscles [2], energy storage [3] and many others [4]. It is well known that PPy can be prepared by either chemical [5] or electrochemical synthesis [6] where different polymeric architectures and properties can be tuned up. Regardless of the intended application of PPy, the presence of dopants to improve its intrinsic physical and chemical properties are required. The use of large dopants such as surfactants is one of the most applied methodology to obtain remarkable stability and electroactive properties [7–9]. The electrochemical synthesis presents interesting advantages if compared to the chemical route, such as short reaction times, limited amount of solvent and chemicals and an easy and reliable control of the film growth and morphology. Simple changes in experimental conditions lead to different electrode interfaces broadening the range of applications and allowing the optimization of diffusional properties [10].

Besides the excellent electrochemical properties of the PPy itself, it is well described in the literature that the synthesis of composites or hybrid materials has been recognized as a useful approach towards improved properties. Thus, hybrids incorporating either inorganic or organic foreign species, such as PPy/AuNPs [11], PPy/Prussian Blue [12], PPy/$Ni(OH)_2$ [13], PPy/natural polymers [14], PPy/carbon nanotubes [15], PPy/graphene [16], among others, have been extensively studied. In general, PPy enhances the electroactivity of the modified electrodes by increasing the conductivity and electroactive properties of the second material which is normally dispersed in the PPy matrix. Another approach to modify the PPy properties is by the addition of a second monomeric unity during the polymerization process, leading to an intercalation in the individual segments alongside the polymeric chain [17]. Among many different candidates to be inserted in the PPy chain, the imidazole (IMZ) molecule appears as a natural choice as their chemical structures are very closely related as shown in Scheme 1.

There are few reports concerning the electrochemical properties of IMZ. In one of these contributions, Wang et al. [18], reported the chemical and electrochemical polymerization of the IMZ in acetonitrile and proposed a mechanism, very similar to PPy. According to these authors, the polymerization occurs by nitrogen bonding under a high voltage (2.8 V), indicating a huge kinetic barrier to form the polymer, if compared to PPy. Huang et al. [19] reported the improvement in the capacitance by tuning the morphology of poly(3,4-ethylenedioxythiophene) (PEDOT) with different proportions of IMZ, that acts as an inhibitor of kinetic polymerization. The specific capacitance of PEDOT was increased from 57 $Fg^{-1}$ to 124 $Fg^{-1}$ (almost 2.2 times larger) due to the presence of IMZ. According to the authors, the PEDOT-IMZ with larger molecular weight enhances the staking of the polymeric chains and brings higher conductivity [19]. In addition, a copolymer based on pyridine and IMZ was reported showing higher conductivity and thermal stability in comparison with poly (pyridine) [20]. Besides, IMZ derivatives have been used in energy storage devices, for example, graphene was functionalized with benzimidazole (BZM), improving the electrode/electrolyte interfacial charge transfer process and enhancing the stability and specific capacitance of the modified electrodes [21]. Hybrid materials based on heteropolyacids containing phosphomolybdic acid (PMO) and 1-butyl-3-methylimidazolium (BMIM) were deposited onto stainless steel by electrophoretic deposition presenting a specific capacitance around 172 $Fg^{-1}$ with 89% capacity retention after 1100 cycles [22].

Supercapacitors are particularly interesting energy storage devices due to their intrinsic characteristic, such as high power and longer cycle life [23–25]. PPy has been frequently used for the development of supercapacitors electrodes, due to its unique features such as fast charge-discharge mechanism, good thermal stability, low cost, and high energy density [26]. It is important to note that the capacitance of PPy is strongly dependent on the ionic diffusion and the film porosity and morphology. Thus, many efforts have been focused on PPy-based modified electrodes, some of them are described as reduced graphene oxide/PPY/$MnO_2$ ternary films with interactive laminated structure [16], nanobelts, nano-bricks and nanosheets of PPy onto stainless steel [27], organic molecules/PPy/MWCNTs by electropolymerization method [28] amongst other.

Herein, we report the direct electrosynthesis of a novel copolymer based on PPy-IMZ. The effect of IMZ/Py ratio on the polymerization reaction was investigated by many different techniques corroborating the presence of IMZ in the PPy chain.

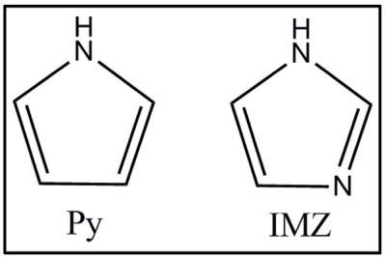


Scheme 1. Structure of the monomers pyrrole (Py) and imidazole (IMZ).

The materials were deeply characterized by spectroscopic, electrochemical and microscopic techniques. Also, the capacitive properties of the PPy-IMZ electrodes were tested.

## 2. Experimental

Sodium dodecylbenzenesulfonate (NaDBS), imidazole and Pyrrole were obtained from Aldrich. Sulfuric acid ($H_2SO_4$) was purchased from Synth. All reagents were used as received except pyrrole, which was distilled prior to use. ultrapurified water (R > 18 MV $cm^{-1}$) was used to prepare the solutions.

The electrode modifications were carried out potentiostatically by applying 0.8 V vs Ag/AgCl/$Cl^-_{sat}$ until the charge passed through the electrode reached 30 mC $cm^{-2}$. This procedure assures the same amount of electroactive material for all modifications. Stainless steel and a large platinum foils were used as working
and counter electrodes respectively. The masses of the active material were obtained by weighing the dried electrodeposited film using a balance with five decimal places, just after the polymerization the modified electrodes were gently washed with deionized water to remove the excess of ions and weakly adsorbed species, then they were placed in a dissecator under room temperature and low pressure and kept overnight. The mass obtained for each electrodeposited material was 0.3 mg. For the depositions, the electrolytes were prepared employing different proportions of the monomers, Py and IMZ, in a 1 mmol $L^{-1}$ NaDBS aqueous solution, with pH = 5 by adjusting with $H_2SO_4$ aliquots. The following electrolytes were used and labeled accordingly to the monomers molar proportions: (i) 50.0 mmol $L^{-1}$ Py (100Py:0IMZ); (ii) 37.5 mmol $L^{-1}$ Py + 12.5 mmol $L^{-1}$ IMZ (75Py:25IMZ); (iii) 25.0 mmol $L^{-1}$ Py + 25 mmol $L^{-1}$ IMZ (50Py:50IMZ) and (iv) 20.0 mmol $L^{-1}$ Py + 30.0 mmol $L^{-1}$ IMZ (40Py:60IMZ). For the polymer/copolymer deposited on the electrode surface, they were nominated p(xPy:yIMZ), where x and y are the molar proportion of the monomers used during the electrosynthesis.

The surface morphological analyses were carried out by Scanning Electron Microscopy (SEM) in a FEI Quanta 450 FEG and at least five different points from three different samples were analyzed, herein we show the representative images. The X-ray photoelectron (XPS) spectra were recorded with a SPECS Germany, PHOIBOS 150. Raman spectra were obtained in a Reninshaw spectrometer using the 533 nm/He-Ne radiation. The electrochemical experiments and electrochemical impedance Spectroscopy (EIS) were performed in a Bio-Logic VMP3 potentiostat. The EIS data were obtained in open circuit potential (OCP) between
100 kHz to 0.01 Hz. All electrochemical measurements were carried out in 1 mol $L^{-1}$ $H_2SO_4$ electrolyte. The experiments were done in triplicate to assure the reproducibility of the results.

## 3. Results and discussion

The influence of IMZ during the electrosynthesis can be observed from data in Fig. 1(a). It is shown the linear voltammetry (lv) of each synthetic solution tested herein. For the solution containing only Py (100Py:0IMZ), the polymerization starts at around 0.5 V, indicating the oxidation of Py at the electrode surface. Furthermore, the current density increases as the potential is scanned to higher values presenting a discrete peak at about 0.7 V, which is a characteristic of the freshly formed PPy and described elsewhere [29–31]. On the other hand, the oxidation of IMZ does not present any increment in the faradaic current, indicating the lack of electroactivity of this molecule in the potential window tested.

The addition of IMZ in Py solution significantly affects the electrosynthesis signal in the lv, which clearly suggests the different growth mechanism for PPy in the presence of IMZ. Two changes are noticed in the lv signals: the first concerns the continuous shift in the oxidation potential of Py towards more positive potential with increasing proportion of IMZ.

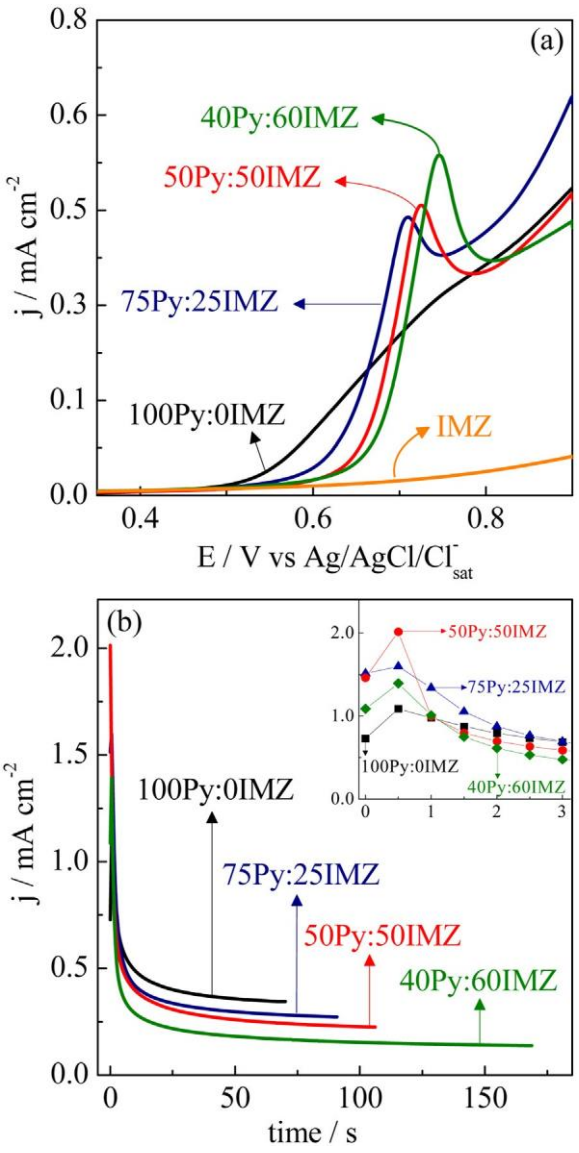


Fig. 1. (a)Linear voltammograms obtained in the synthetic solutions containing different proportions of pyrrole and imidazole, scan rate of 10 mV $s^{-1}$. (b) Chronoamperograms obtained during the electrodeposition of PPy-IMZ in different proportions, the insert represents the early stages of the polymerization. The depositions were carried out at 0.8 V by controlling the charge passed through the electrode (30 mC $cm^{-2}$).

The second one is related to the appearance of a well-defined oxidation peak. The oxidation peaks can be found at 0.71, 0.73 and 0.75 V in the 75Py:25IMZ, 50Py:50IMZ and 40Py:60IMZ samples, respectively. These facts indicate that the IMZ affects both kinetic and diffusional processes of the Py and PPy oxidation. The increase in the kinetic barrier was also observed in the PEDOT formation [19], although there was no definitive conclusion in which way the presence of IMZ retards the polymerization reaction. One possible explanation can be raised in terms of the diminishment of the Py molecules in the surroundings of the fresh formed radicals, thereby slowing down the PPy polymerization, as commented in other works [6,32,33]. If the formed radicals have a longer lifetime, they can react with IMZ molecules producing dimer radicals and continuing the polymerization reaction or even interrupting the polymerization, as will be discussed later on. Assuming the formation of a first layer of PPy-IMZ, this one is surely less electroactive than the pristine PPy, which also helps to slow down the electrochemical polymerization. This fact allied to the lower amount of Py monomers in the bulk solution agrees with the shifting and the more definition of the Py oxidation peak with the increase of IMZ proportion in the synthetic solution, experimentally observed.

In order to further investigate the mechanism for the PPy:IMZ copolymer formation, the electrodes were potentiostatically modified at 0.8 V, which is the region with no kinetic limitation. The chronoamperograms obtained during the electrodepositon are shown in Fig. 1(b). It is possible to observe the increase in the deposition time with the IMZ proportion and the profiles obtained were similar with other analogous synthesis of PPy described elsewhere [34–37]. Accordingly to Licona-Sanzhezet al. [37], the shape of the polymerization curve can be attributed to both simultaneous reaction at the electrode surface, also called as multiple hemispherical 3D-nucleation and to the PPy nucleation and grown in the surface of the new phase freshly formed. Using the model proposed [37], we obtained the density of the active sites on the electrode surface: $1.80 \times 10^9$, $0.52 \times 10^9$, $0.36 \times 10^9$ and $0.21 \times 10^9$ $cm^{-2}$ for 100Py:0IMZ, 75Py:25IMZ, 50Py:50IMZ and 40Py:60IMZ electrodes, respectively. These results indicated that the active sites on the electrode surface for polymerization of Py is around 88% lower for 40Py:60IMZ than for 100Py:0IMZ sample. This suggests that the cation radical of Py is reacting with the protonated IMZ, leading to the formation of a less reactive dimer ($[Py - IMZ]^{\bullet+}$), thus, more time for the electrodeposition of the same amount of charge is necessary, also, depicting the early stages of the polymerization, a maximum of the chronoamperometric curves are present indicating a

nucleation step [6,32]. These results agree with previous cyclic voltammetry analysis. Also, it is important to note that IMZ presented no electroactivity, therefore the observed faradaic current can be attributed solely to the Py oxidation at the electrode surface. By this way, it is interesting to provide similar conditions for the electropolymerization of the Py: IMZ samples, so all electrodes were modified potentiostatically, as it is possible to control the amount of charge passed through the electrode, providing by this way similar amounts of electroactive material.

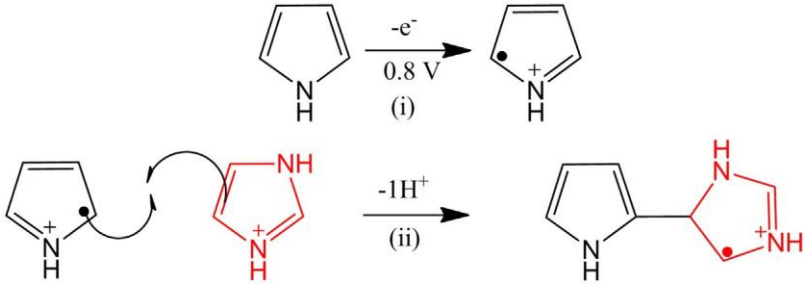


Fig. 2. Proposed mechanism for the $[Py\text{-}IMZ]^{+\bullet}$ radical formation.

As commented earlier, there are very few works in literature which describe the electrochemical behavior of IMZ molecules, nevertheless, we can propose a mechanism of electropolymerization based on the changes observed in Fig. 1 and adopting a direct comparison with the PPy formation, since the monomers are highly alike, the reaction mechanism should be similar as well. The PPy polymerization is well established, which combines both electrochemical and chemical steps [6,32]. The applied potential at the electrode interface promotes the Py oxidation to the radical cation $(C_4H_5N)^{+\bullet}$ (Fig. 2, step (i)) but as observed in Fig. 1(a), even at high voltages, IMZ does not present any current signal, thus in the presence of $Py^{+\bullet}$ and protonated IMZ, a radical dimer $[Py-IMZ]^{+\bullet}$ is formed, Fig. 2(ii). This reaction can occur any time during the synthesis since the electrode is constantly polarized at 0.8 V, therefore more radicals or even oligomer radicals can be found.

According to Aldabbaghet al., the radical cyclization of n-alkylimidazoles is regioselective, favoring the reaction in the C5-position rather than the C2-position [38].Therefore, we believe that the reaction with protonated IMZ occurs at the C5 position followed by reaction with another $Py^{+\bullet}$. Fig. 3 shows the reaction between a Py-tetramer radical with IMZ protonated. The reaction can follow two different ways: the oligomer containing IMZ can react with other $Py^{+\bullet}$ leading to the insertion of the IMZ along the chain (Fig. 3 (step i)) and by the loss of two $H^+$, the aromaticity of the molecules is restored. The second route is the reaction of the oligomer containing IMZ radical with the radical dimer $[Py-IMZ]^{+\bullet}$, resulting in the insertion of two IMZ molecules in sequence in the polymer chain (Fig. 3 (step ii)). The last one might result in a less reactive structure, diminishing by this way the actives sites to continue the polymerization on the electrode surface, as observed during the kinetics studies.

Furthermore, the oligomers containing Py-IMZ can oxidize and react with Py or $Py:IMZ^{+\bullet}$ resulting in the growth of the copolymer. Further, the results herein suggest that different amounts of IMZ molecules could be inserted in the polymeric chain, as will be discussed in the XPS analysis. The presence of the IMZ in different positions alongside the polymeric chain could orientate the growth resulting in a copolymer with different branching, that could contribute to changes in the final morphology of the material [39,40]. Following the same mechanism described below, the quantity of IMZ presented in the copolymer can be different by repetition the steps i or ii as is shown in Fig. 3. In fact, more evidences are necessary to confirm the steps of the copolymerization mechanism, however, we believe that the IMZ react with the PI resulting in a copolymer with similar structures showed in Fig. 3. According to the IMZ proportion during the electrosynthesis, different amounts of IMZ can be inserted in the copolymer (steps i or ii), as will be discussed in the XPS and Raman studies. Also, when the reaction occurs with the $Py:IMZ^{+\bullet}$ radical (step ii) the oligomer tends to be less reactive and the electrodeposition process to reach at the same charge requires more time, as discussed in the kinetics studies.

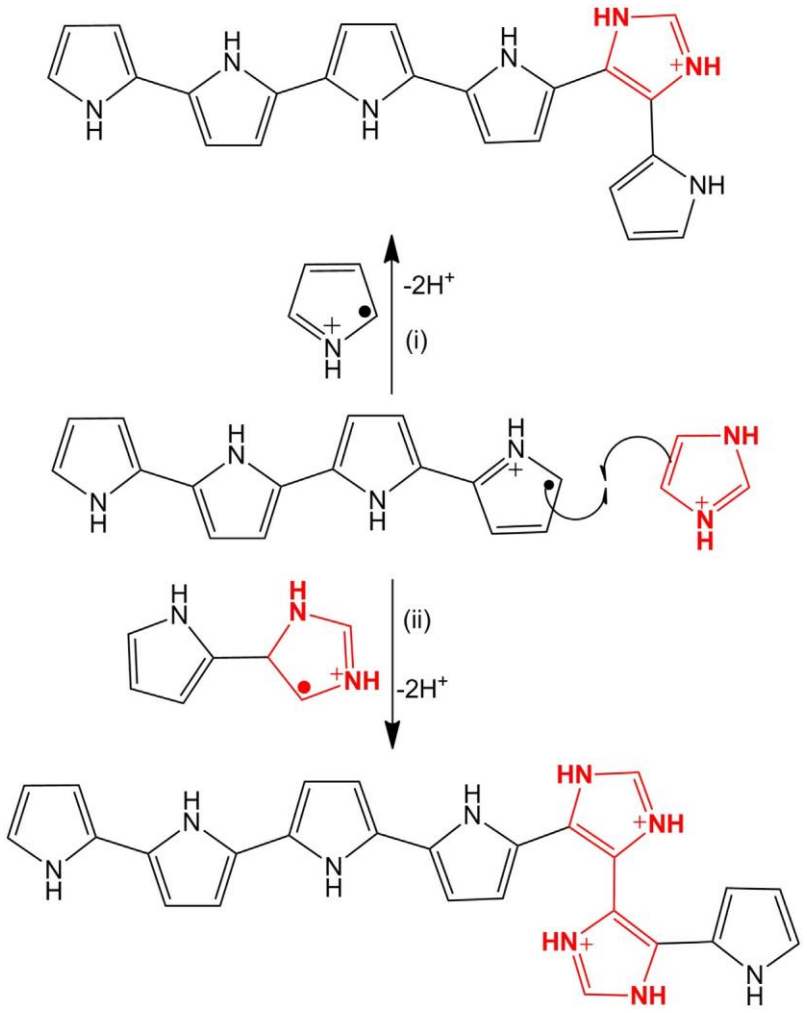


Fig. 3. Mechanism of the copolymerization of p(Py:IMZ).

In order to investigate the influence of the copolymerization process on the morphology of the materials, SEM images were obtained from electrodes modified with the different proportions of Py:IMZ (Fig. 4). The p(100Py:0IMZ) modified electrode (Fig. 4(a)) showed the typical globular structure of PPy doped with $DBS^-$ anions [37,41,42], however in the presence of IMZ, the morphologies presented different patterns. By increasing the amount of IMZ in the synthetic solution, observed in the p(75Py:25IMZ) and p (50Py:50IMZ) samples (Fig. 4(b) and (c), respectively), the globular morphology is observed, nevertheless, comparing with the other electrodes, the globules are clearly larger with no specific shape, besides in the p(50Py:50IMZ) sample some smaller structures are observed (shown in more detail in Fig. 4(c1)), these structures were directly grown on the top of the globules.

At this point, it is very hard to define the chemical identity of these structures. Nevertheless, the deposition mechanism clearly suffers a drastic change as both kinetic and diffusional processes are influenced by the change in the proportion of the species at the electrode interface and the different radical structures that are present at the electrode surface. This characteristic is deeply pronounced in the p(40Py:60IMZ) sample (Fig. 4(d)). Indeed, the obtained morphology is completely different than the later ones with no globular pattern nor smaller structures. Instead, interconnected structures with no specific shape are found. It is possible to see that a lot of branches are well spread over the entire surface of the electrode. These branches are shown in more detail in Fig. 4(d1).

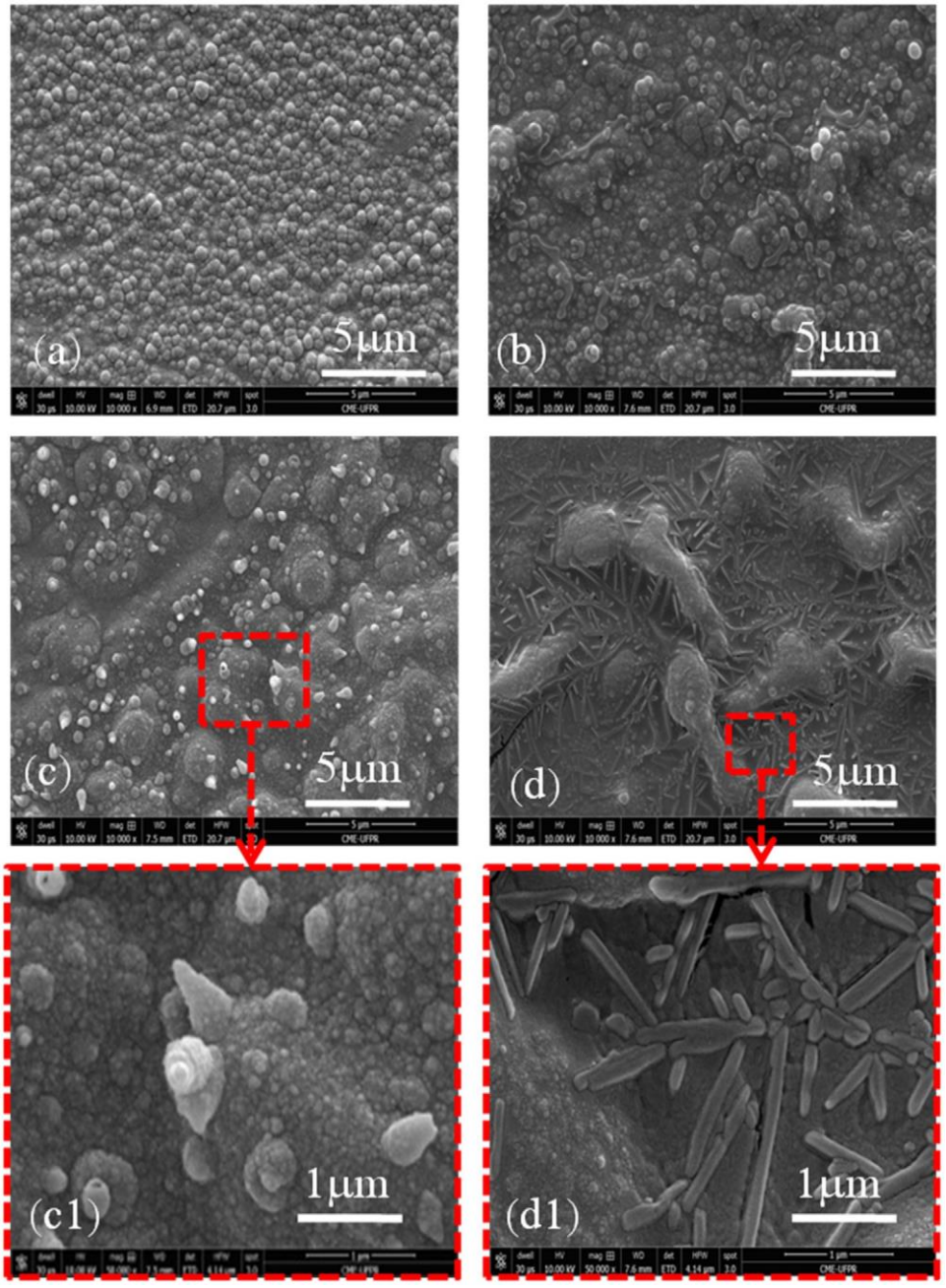


Fig. 4. Representative SEM images of the electrodes surface obtained at 0.8 V with control of deposition charge (30 mC $cm^{-2}$), synthesized in different proportions of Py:IMZ. (a) p(100Py:0IMZ), (b) p(75Py:25IMZ), (c) and (c1) p(50Py:50IMZ), (d) and (d1) p(40Py:60IMZ).

So far, it is evident that the presence of IMZ clearly affects the electrochemical oxidation of Py at the electrode surface producing different electrode morphologies and the copolymer formation depends on the proportion of Py:IMZ used in the synthetic solution. Nevertheless, it is important to investigate if the stoichiometry composition of the polymeric deposit is directly related with the one used during synthesis. Though, the precise determination of the amount of Py and IMZ in the copolymer electrodeposited is not a simple task as the chemical identities of Py and IMZ are very alike and the unique difference between them is the nucleophilic nitrogen present in the IMZ molecule. To investigate this issue, XPS experiments were performed. The results are shown in Fig. 5 for the p(100Py:0IMZ) and p (40Py:60IMZ) samples. Due to the similarities, the other samples and the full spectra are shown in the supplementary material S1.

The complete XPS spectra of the samples show the very same pattern, presenting the characteristic peaks of N1 s (rv400.5 eV), C1 s (rv284.7 eV) attributed to N in the polymer backbone and the peak of O1 s (rv533 eV) assigned to the surface oxidation of PPy (supplementary material S1) [8,43]. In Fig. 5(a) the deconvolution spectra of the N1 s signal of the p(100Py:0IMZ) sample is shown, revealing three components with different contribution and four components for the p(40Py:60IMZ) sample, Fig. 5(b), also observed in the p(75Py:25IMZ) and p(50Py:50IMZ) samples (supplementary information S1).

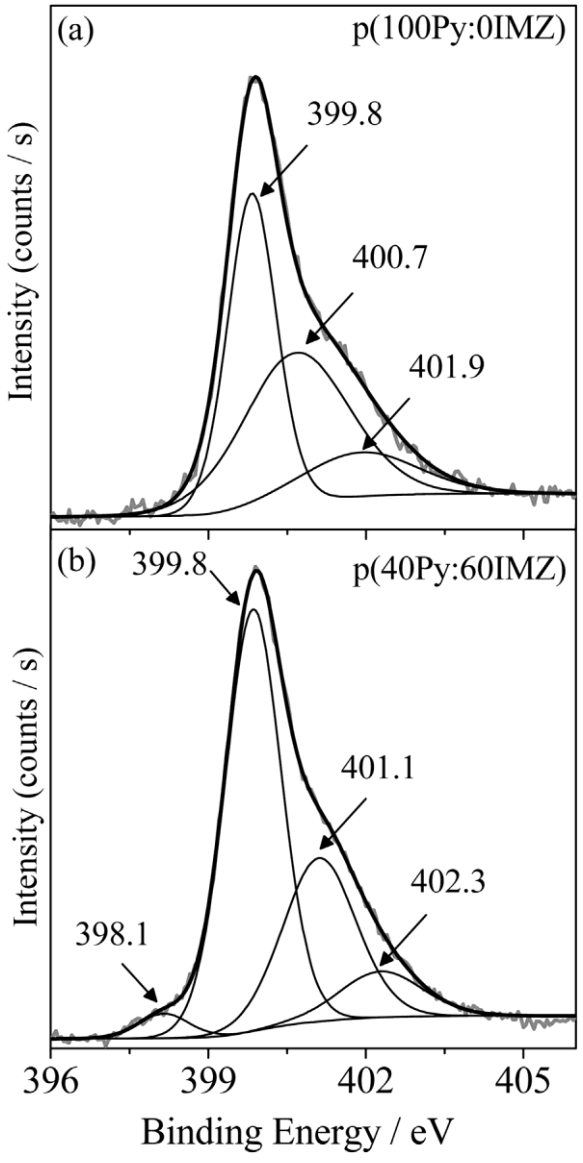


Fig. 5. XPS spectra of (a) p(100Py:0IMZ) and (b) p(40Py:60IMZ) modified electrodes in the N1 s peak region.

The N1 s components at 398.1, 399.8, 401.1 and 402.4 eV are attributed to quinoid imine (C=N), benzenoid imine (-NH), protonated benzenoid imine (—$NH^+$—) and protonated quinoid imine (=$NH^+$ –), respectively [8]. Interestingly, the absence of a component at 402.4 eV in p(100Py:0IMZ) sample, suggests that IMZ contributes to a higher oxidation level of the PPy, since this contribution is associated to the bipolaron structure of PPy [43]. The presence of protonated IMZ in the copolymer could contribute to the intensity of the (=$NH^+$ –) bond and also the oxidized state of the copolymer. The quinoid imine peak (398.1 eV) appears only in those IMZ containing samples, indicating its insertion in the polymeric backbone [44,45]. In addition, the increase of the nitrogen amount in the material and the increment on the proportion between quinoid and neutral bonding (=NH/—NH) (Table 1), corroborating the presence of IMZ.

As suggested by the XPS analyses, the materials present both structures of neutral and oxidized states of the copolymer, which can be attributed to either the presence of defects in the polymer chain and the combination of different length intervals [46]. In order to further investigate this issue, vibrational spectra of the samples were obtained, Fig. 6. In general, as observed in XPS, the Raman spectra of the copolymers p(Py:IMZ) are very similar with the pristine p(100Py:0IMZ) and previous studies described elsewhere [46,47] although, some interesting features are observed as follow: i) the band around 1590 $cm^{-1}$ in the p (100Py:0IMZ) sample is shifted around 10 $cm^{-1}$ to higher frequencies in the p(Py:IMZ) samples, this shifting is attributed to the higher oxidation states of PPy [46–48] ii) the bands around 1050 and 1080 $cm^{-1}$ result from vibrations of the oxidized and reduced states of PPy, respectively [46,48,49]. From the deconvolution of these bands it is possible to determine the oxidation level of the material by the ratio between the signals (1050/1080 $cm^{-1}$) (supplementary material S2). The values found for each sample are shown in Table 1, indicating that the p(40Py:60IMZ) samples have 3.2-fold higher oxidation level than the PPy, corroborating the XPS analysis; iii) the band at 1530 $cm^{-1}$ is attributed to the C-N vibrations (red circle in Fig. 6) [49], which presents higher intensity in the p(50Py:50IMZ) and p(40Py:60IMZ) samples suggesting that IMZ molecules were inserted in the material and a copolymer was obtained. This is according with the increment of the nitrogen amount in the IMZ containing samples, observed in the XPS studies (Table 1).

The electroactivity of the modified electrodes was evaluated by cyclic voltammograms, shown in Fig. 7. It is important to note that all electrodes were very stable with no changes in the voltam metric behavior under continuous cycling (250 cycles were tested), in Fig. 7(a) are presented the 10th cycle of each experiment. As it is possible to observe, all samples present a rectangular shape with discrete redox peaks, suggesting the pseudocapacitive behavior [26,50]. Apparently, there is no direct connection between the IMZ proportion with the peak position. In the presence of IMZ in the polymeric backbone, a more defined oxidation wave and more reversible behavior in terms of $\Delta E_{peak}$ are observed. These electrochemical features seem to be more related to diffusional processes rather than any ease electron transfer at the electrode surface, so the changes of the morphology at the electrode interface (as observed in SEM experiments) by the incorporation of IMZ plays an important role in the voltammetric behavior of the modified electrodes. Also, to the best of our knowledge, there is no similar system in literature to compare with, which at this point becomes very tricky any complete elucidation of this point. In Fig. 7(b) are shown the voltammetric cycles under different scan rates of the p(50Py:50IMZ) modified electrode. As it can be seen, there is no peak shifting even in a faster scan rates, corroborating the remarkable electrochemical reversibility observed. It is important to note that the other modified electrodes containing IMZ presented similar results (supplementary material S3).

Table 1
Results obtained from XPS and Raman analysis to the p(Py:IMZ) modified electrodes.

| Modified electrode | C % | N % | O % | =NH/—NH % | Ratio of the area of the Raman bands (1080 $cm^{-1}$/1 |
|---|---|---|---|---|---|
| p(100Py:0IMZ) | 83.8 | 5.8 | 10.4 | 0 | 1.0 |
| p(75Py:25IMZ) | 82.7 | 8.1 | 9.2 | 4.5 | 2.7 |
| p(50Py:50IMZ) | 83.0 | 9.1 | 7.9 | 5.9 | 2.7 |
| p(40Py:60IMZ) | 82.6 | 8.5 | 8.9 | 6.3 | 3.2 |

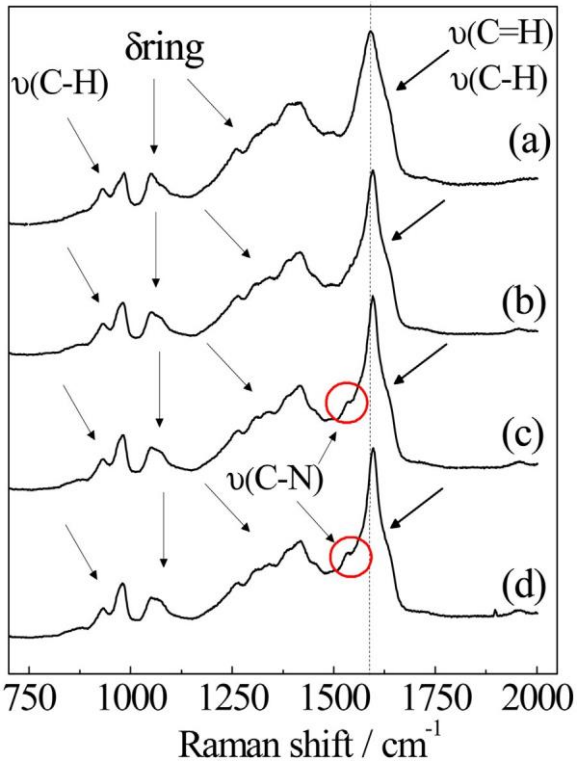


Fig. 6. Raman spectra recorded for the modified electrodes, synthesized employing different proportions of Py:IMZ: (a) p(100Py:0IMZ), (b) p(75Py:25IMZ), (c) p(50Py:50IMZ) and (d) p(40Py:60IMZ), $\lambda_0$ = 540 nm.

As observed in the voltammetric studies, the modified electrodes present a high capacitive component, so the study of this property aiming the development of energy storage electrodes becomes an interesting perspective. To do so, the specific capacitances of the modified electrodes were calculated as follows [51]:

$$C_m = \frac{1}{m\nu(Vc - Va)} \int_{Va}^{Vc} I(V)dV \qquad (1)$$

where, $C_m$ is the specific capacitance ($Fg^{-1}$), $\nu$ is the scan rate ($mV\ s^{-1}$), $V_c$ and $V_a$ are the potential limits of the voltammetric scan (0 up to 0.7 V), I is the response current (mA) and m is the mass of the active material. This methodology was applied for all the modified electrodes and the results are shown in Fig. 8(a).

The specific capacitance drops significantly with the increase of the scan rate, as expected for pseudocapacitive materials as a consequence of the slow Faradaic reaction at faster scan rates, that does not allow the complete ion intercalation in the microporous structures [50]. In all the scan rates tested, the p(50Py:50IMZ) modified electrode showed the highest value of specific capacitance, which agrees with the voltammetric behavior shown in Fig. 7(a). The improvement can be associated to the discussion previously made by XPS and Raman, i.e., the higher oxidation level of the polymer improves the conductive and capacitive properties of the copolymer[46]. Also, the SEM images showed the more organized morphology of the p(50Py:50IMZ) sample suggesting that the IMZ affect the polymer growth on the electrode surface resulting in enhanced properties. Considering the specific capacitance values of the p(50Py:50IMZ) electrode (201 $F\ g^{-1}$) it presents comparable performance with PPy electrodes obtained by electrodeposition onto carbon cloth electrodes, which have a higher surface area due the porous electrode geometry (236 $F\ g^{-1}$) [52] and higher than PEDOT electrodes (124 $F\ g^{-1}$) using IMZ as inhibitor of the polymerization reaction [19].

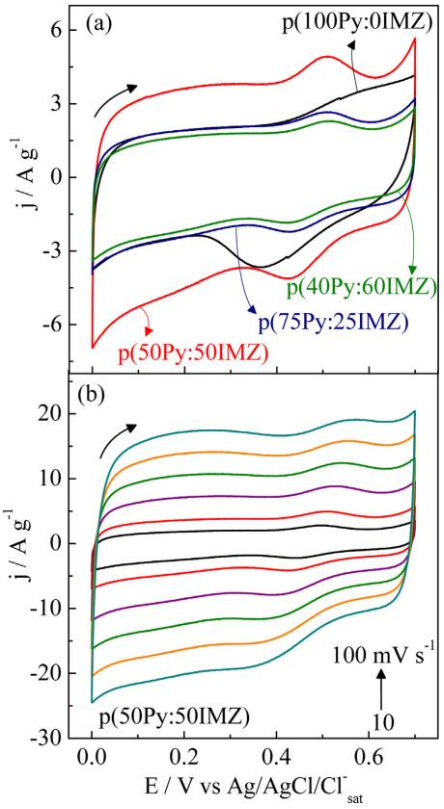


Fig. 7. (a) CV curves of the modified electrodes at scan rate of 20 $mVs^{-1}$ (b) Voltammograms of the p(50Py:50IMZ) modified electrode at different scan rates, electrolyte $H_2SO_4$ 1 mol $L^{-1}$.

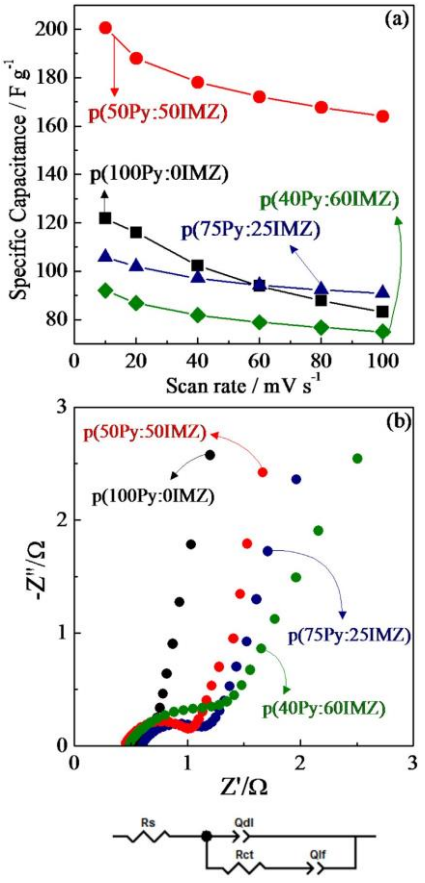


Fig. 8. (a) Specific capacitances obtained from the modified electrodes, by the voltammetric study. (b)Nyquist plot of the p(PY:IMZ) electrodes obtained in open potential circuit in $H_2SO_4$ 1 mol $L^{-1}$ as electrolyte;.

To further study the electrochemical interface of the p(Py:IMZ) modified electrodes, EIS experiments were carried out and the results are found in Fig. 8(b), it is shown the Nyquist plots, it is observed that all samples presented a typical conducting polymer EIS response, i.e., a semicircle at the high frequency region due to the Faradaic process at the electrode/electrolyte interface and a straight line at the low frequency region related to the amount of intercalated charge in the polymer film upon oxidation process in order to maintain charge neutrality [53,54]. The discussion of the results will be presented in terms of the study of the presented equivalent circuit modeling (Fig. 8), composed by a series resistance ($R_s$) that accounts for the ohmic resistance of the film, electrolyte and current collectors [55], a charge-transfer resistance ($R_{ct}$), related to the interfacial Faradaic process, a constant phase element ($Q_{dl}$), accounting for the double-layer capacitance, and another constant phase element ($Q_{lf}$) relating the amount of intercalated charge at the polymeric film in order to maintain charge neutrality. The calculated values of the equivalent circuit are presented in Table 2.

Table 2
Parameters calculated from EIS analysis from p(PPy:IMZ) modified electrodes.

| Modified electrode | $R_S$/V | $R_{ct}$/V | $Q_{dl}$/F $s^{n-1}$ | $Q_{lf}$/F $s^{n-1}$ |
|---|---|---|---|---|
| p(100Py:0IMZ) | 0.50 | 0.21 | 0.0041 | 0.0095 |
| p(75Py:25IMZ) | 0.60 | 0.72 | 0.0033 | 0.026 |
| p(50Py:50IMZ) | 0.45 | 0.70 | 0.0022 | 0.045 |
| p(40Py:60IMZ) | 0.50 | 1.00 | 0.0033 | 0.022 |

Considering that the same current collectors and electrolyte were used in all experiments, the $R_s$ values will be directly related to the electronic transport at the polymeric film [56]. It was observed that the p(50Py:50IMZ) electrode presented the lowest value, suggesting that the electron transport is favored for this copolymer. The charge-transfer resistance ($R_{ct}$) values confirms the early discussion where the addition of IMZ in the polymericfilm is somehow hindering the charge-transfer process at the electrode/ electrolyte interface probably by the lack of electroactivity of the IMZ molecule, where any redox reaction at the polymer interface should be less pronounced. It is important to point out that the apparent lack of electroactivity does not damage the supercapacitive properties of the modified electrode, where other EIS parameters can be discussed [57,58].

The double-layer capacitance was evaluated by the constant phase element ($Q_{dl}$) that is related to the electrode/electrolyte interface area. Accordingly to our calculations, the p(100Py:0IMZ) modified electrode presented the highest electrode/electrolyte interface electroactive area. It is noticeable that the formation of the copolymer diminishes the $Q_{dl}$ values, which is related to a change in the film morphology [59,60], as depicted by the SEM images. The low-frequency capacitance was evaluated by the constant phase element ($Q_{lf}$), while the increase of the $Q_{lf}$ values for the modified electrodes in the presence of IMZ shows that the load of intercalated charge has increased in the polymeric film, also observed by the Raman spectra. These facts agree with the increase of the pseudocapacitance behavior of the IMZ modified electrodes and the conductive form of the PPy, where the highest value was found for the p(50Py:50IMZ) electrode, corroborating the best supercapacitive properties evaluated by cyclic voltammograms.

## 4. Conclusions

We have successfully prepared nanostructured copolymersofPy and IMZ by electrodeposition method. SEM images showed that IMZ induces changes in the process. In addition, the kinetic studies indicated that the presence of IMZ decreases in 88% the active sites for copolymerization on the electrode surface, leading to different electrodes morphologies. Also, XPS and Raman analyses revealed that IMZ improves the oxidation level of the copolymer, resulting in an improvement of the conductive and capacitive properties of the material. In addition, our results suggest the formation of a copolymer based on PPy:IMZ which makes this material interesting to use for a variety of different applications, for example, as electrochemical sensors, catalysts, protein separation and energy storage devices. Also, we have proposed for the first time an electrochemical mechanism for the copolymerization between Py and IMZ. Our electrochemical studies revealed that, depending of the IMZ amount in the copolymer, specific capacitance can be improved from 122 F $g^{-1}$p(100Py:0IMZ) to 201 F $g^{-1}$p (50Py:50IMZ) (61%) at 10 mV $s^{-1}$. Also, the EIS studies have allowed us to show how a synergetic effect between Py and IMZ contributes to reach these superior pseudocapacitive properties.

## Acknowledgments

The author (FW) gratefully acknowledge financial support from CAPES Foundation Process BEX 3196/14-3. DPD acknowledges Marie-Curie funding through Beatriu de Pinos Program (BP-DGR-2013) from the Catalan system of science and technology, Spain and University of Adelaide Research Fellowship, Australia. Partial funding from MINECO-FEDER (MAT2015-68394) and AGAUR (NESTOR 2014_SGR_1505) is acknowledged. ICN2 acknowledges support of the Spanish MINECO through the Severo Ochoa Centers of Excellence Program under Grant SEV-2013-0295. Also, the financial support from UFPR, CNPq, CAPES, L'Oréal-UNESCO-ABC, Fundação Araucária and National Institute of Science and Technology of Carbon Nanomaterials (INCT-Nanocarbon).

## Appendix A. Supplementary data

Supplementary data associated with this article can be found, in the online version, at http://dx.doi.org/10.1016/j.electacta.2017.05.082

## References


[1] I.M. Apetrei, C. Apetrei, Amperometric biosensor based on polypyrrole and tyrosinase for the detection of tyramine in food samples, Sensor. Actuat. B Chem. 178 (2013) 40.

[2] M. Fuchiwaki, J.G. Martinez, T.F. Otero, Asymmetric Bilayer Muscles. Cooperative and Antagonist Actuation, Electrochim. Acta 195 (2016) 9.

[3] Y. Shi, L. Peng, Y. Ding, Y. Zhao, G. Yu, Nanostructured conductive polymers for advanced energy storage, Chem. Soc. Rev. 44 (2015) 6684.

[4] Z.B. Huang, G.F. Yin, X.M. Liao, J.W. Gu, Conducting polypyrrole in tissue engineering applications, Front, Mat. Sci. 8 (2014) 39.

[5] Y. Tan, K. Ghandi, Kinetics and mechanism of pyrrole chemical polymerization, Synth. Met. 175 (2013) 183.

[6] S. Sadki, P. Schottland, N. Brodie, G. Sabouraud, The mechanisms of pyrrole electropolymerization, Chem. Soc. Rev. 29 (2000) 283.

[7] T.D. Licona-Sanchez, G.A. Alvarez-Romero, M. Palomar-Pardave, C.A. Galan- Vidal, M.E. Paez-Hernandez, M.T.R. Silva, M. Romero-Romo, Influence of the Cation Nature of the Sulphate Salt on the Electrochemical Synthesis of Sulfate- Doped Polypyrrole, Int. J. Electrochem. Sc. 6 (2011) 1537.

[8] N. Su, H.B. Li, S.J. Yuan, S.P. Yi, E.Q. Yin, Synthesis and characterization of polypyrrole doped with anionic spherical polyelectrolyte brushes, Express Polym. Lett. 6 (2012) 697.

[9] Q. Wen, X. Pan, Q.-x. Hu, S.-j. Zhao, Z.-f. Hou, Q.-z. Yu, Structure-property relationship of dodecylbenzenesulfonic acid doped polypyrrole, Synth. Met. 164 (2013) 27.

[10] M. Palomar-Pardave, B.R. Scharifker, E.M. Arce, M. Romero-Romo, Nucleation and diffusion-controlled growth of electroactive centers – Reduction of protons during cobalt electrodeposition, Electrochim. Acta 50 (2005) 4736.

[11] E. Spain, T.E. Keyes, R. Forster, Polypyrrole-gold nanoparticle composites for highly sensitive DNA detection, Electrochim. Acta 109 (2013) 102.

[12] N.V. Talagaeva, E.V. Zolotukhina, P.A. Pisareva, M.A. Vorotyntsev, Electrochromic properties of Prussian blue-polypyrrole composite films in dependence on parameters of synthetic procedure, J. Solid State Electrochem. 20 (2016) 1235.

[13] F. Wolfart, D.P. Dubal, M. Vidotti, P. Gomez-Romero, Hybrid core-shell nanostructured electrodes made of polypyrrole nanotubes coated with Ni(OH) 2 nanoflakes for high energy-density supercapacitors, RSC Adv. 6 (2016) 15062.

[14] S. Yalcinkaya, C. Demetgul, M. Timur, N. Colak, Electrochemical synthesis and characterization of polypyrrole/chitosan composite on platinum electrode: Its electrochemical and thermal behaviors, Carbohyd. Polym. 79 (2010) 908.

[15] Y.L. Chen, L.H. Du, P.H. Yang, P. Sun, X. Yu, W.J. Mai, Significantly enhanced robustness and electrochemical performance of flexible carbon nanotube- based supercapacitors by electrodepositing polypyrrole, J. Power Sources 287 (2015) 68.

[16] H.Y. Zhou, Z. Yan, X. Yang, J. Lv, L.P. Kang, Z.H. Liu, RGO/MnO2/polypyrrole ternary film electrode for supercapacitor, Mater. Chem. Phys. 177 (2016) 40.

[17] M.C. Clochard, C. Baudin, N. Betz, A. Le Moel, C. Bittencourt, L. Houssiau, J.J. Pireaux, D. Caldemaison, New sulfonated pyrrole and pyrrole 3-carboxylic acid copolymer membranes via track-etched templates, React. Funct. Polym. 66 (2006) 1296.

[18] H.L. Wang, R.M. O'Malley, J.E. Fernandez, Electrochemical and Chemical Polymerization of Imidazole and Some of Its Derivatives, Macromolecules 27 (1994) 893.

[19] J.H. Huang, C.W. Chu, Achieving efficient poly(3,4-ethylenedioxythiophene)- based supercapacitors by controlling the polymerization kinetics, Electrochim. Acta 56 (2011) 7228.

[20] V. Raj, D. Madheswari, M. Mubarak Ali, Chemical synthesis, characterization, and properties of conducting copolymers of imidazole and pyridine, J. Appl. Polym. Sci. 124 (2012) 1649.

[21] W. Ai, W. Zhou, Z. Du, Y. Du, H. Zhang, X. Jia, L. Xie, M. Yi, T. Yu, W. Huang, Benzoxazole and benzimidazole heterocycle-grafted graphene for high- performance supercapacitor electrodes, J. Mater. Chem. 22 (2012) 23439.

[22] M. Ammam, J. Fransaer, Ionic Liquid–Heteropolyacid: Synthesis, Characterization, and Supercapacitor Study of Films Deposited by Electrophoresis, J. Electrochem. Soc. 158 (2011) A14.

[23] A. Vlad, N. Singh, C. Galande, P.M. Ajayan, Design Considerations for Unconventional Electrochemical Energy Storage Architectures, Adv. Energy Mater. 5 (2015) 1402115.

[24] P. Simon, Y. Gogotsi, Materials for electrochemical capacitors, Nat. Mater. 7 (2008) 845.

[25] D.P. Dubal, O. Ayyad, V. Ruiz, P. Gomez-Romero, Hybrid energy storage: the merging of battery and supercapacitor chemistries, Chem. Soc. Rev. 44 (2015) 1777.

[26] I. Shown, A. Ganguly, L.-C. Chen, K.-H. Chen, Conducting polymer-based flexible supercapacitor, Energy Sci. Eng. 3 (2015) 2.

[27] D.P. Dubal, S.H. Lee, J.G. Kim, W.B. Kim, C.D. Lokhande, Porous polypyrrole clusters prepared by electropolymerization for a high performance supercapacitor, J. Mater. Chem. 22 (2012) 3044.

[28] S. Chen, I. Zhitomirsky, Influence of dopants and carbon nanotubes on polypyrrole electropolymerization and capacitive behavior, Mater. Lett. 98 (2013) 67.

[29] C.M. Li, C.Q. Sun, W. Chen, L. Pan, Electrochemical thin film deposition of polypyrrole on different substrates, Surf. Coat. Technol. 198 (2005) 474.

[30] J. Tietje-Girault, C. Ponce de León, F.C. Walsh, Electrochemically deposited polypyrrole films and their characterization, Surf. Coat. Technol. 201 (2007) 6025.

[31] M. Bazzaoui, J.I. Martins, S.C. Costa, E.A. Bazzaoui, T.C. Reis, L. Martins, Sweet aqueous solution for electrochemical synthesis of polypyrrole: Part 2. On ferrous metals, Electrochim. Acta 51 (2006) 4516.

[32] E.M. Genies, G. Bidan, A.F. Diaz, Spectroelectrochemical study of polypyrrole films, J. Electroanal. Chem. Interfacial Electrochem. 149 (1983) 101.

[33] B.R. Scharifker, E. Garciapastoriza, W. Marino, The growth of polypyrrole films on electrodes, J. Electroanal. Chem. 300 (1991) 85.

[34] F. Wolfart, D.P. Dubal, M. Vidotti, R. Holze, P. Gomez-Romero, Electrochemical supercapacitive properties of polypyrrole thin films: influence of the electropolymerization methods, J. Solid State Electrochem. 20 (2016) 901.

[35] T.F. Otero, E. De Larreta, Electrochemical control of the morphology, adherence, appearance and growth of polypyrrole films, Synth. Met. 26 (1988) 79.

[36] T.F. Otero, M. Alfaro, Oxidation kinetics of polypyrrole films: Solvent influence, J. Electroanal. Chem. 777 (2016) 108.

[37] T.d.J. Licona-Sanchez, G.A. Alvarez-Romero, L.H. Mendoza-Huizar, C.A. Galan- Vidal, M. Palomar-Pardave, M. Romero-Romo, H. Herrera-Hernandez, J. Uruchurtu, J.M. Juarez-Garcia, Nucleation and Growth Kinetics of Electrodeposited Sulfate-Doped Polypyrrole: Determination of the Diffusion Coefficient of SO42- in the Polymeric Membrane, J. Phys. Chem. B 114 (2010) 9737.

[38] F. Aldabbagh, W.R. Bowman, E. Mann, Oxidative radical cyclisations onto imidazoles and pyrroles using Bu3SnH, Tetrahedron Lett. 38 (1997) 7937.

[39] M. Trollsås, M.A. Kelly, H. Claesson, R. Siemens, J.L. Hedrick, Highly Branched Block Copolymers: Design Synthesis, and Morphology, Macromolecules 32 (1999) 4917.

[40] R. Adhikari, G.H. Michler, Influence of molecular architecture on morphology and micromechanical behavior of styrene/butadiene block copolymer systems, Prog. Polym. Sci. 29 (2004) 949.

[41] B.C. Thompson, S.E. Moulton, R.T. Richardson, G.G. Wallace, Effect of the dopant anion in polypyrrole on nerve growth and release of a neurotrophic protein, Biomaterials 32 (2011) 3822.

[42] R. Paisal, R. Martínez, J. Padilla, A.J.F. Romero, Electrosynthesis and properties of the polypyrrole/dodecylbenzene sulfonate polymer. Influence of structural micellar changes of sodium dodecylbenzene sulfonate at high concentrations, Electrochim. Acta 56 (2011) 6345.

[43] L. Ruangchuay, J. Schwank, A. Sirivat, Surface degradation of alpha- naphthalene sulfonate-doped polypyrrole during XPS characterization, Appl. Surf. Sci. 199 (2002) 128.

[44] M.-Y. Hua, H.-C. Chen, R.-Y. Tsai, C.-S. Lai, A novel polybenzimidazole-modified gold electrode for the analytical determination of hydrogen peroxide, Talanta

85 (2011) 631.
[45] W. Liu, K.L. Koh, J. Lu, L. Yang, S. Phua, J. Kong, Z. Chen, X. Lu, Simultaneous catalyzing and reinforcing effects of imidazole-functionalized graphene in anhydride-cured epoxies, J. Mater. Chem. 22 (2012) 18395.
[46] M.J.L. Santos, A.G. Brolo, E.M. Girotto, Study of polaron and bipolaron states in polypyrrole by in situ Raman spectroelectrochemistry, Electrochim. Acta 52 (2007) 6141.
[47] I. Rawal, A. Kaur, Synthesis of mesoporous polypyrrole nanowires/ nanoparticles for ammonia gas sensing application, Sens. Actuators, A 203 (2013) 92.
[48] Y. Furukawa, S. Tazawa, Y. Fujii, I. Harada, Raman-spectra of polypyrrole and its 2,5-C-13-substituted and c-deuterated analogs in doped and undoped states, Synth. Met. 24 (1988) 329.
[49] S.J. Vigmond, V. Ghaemmaghami, M. Thompson, Raman and resonance raman- spectra of polypyrrole with application to sensor – gas probe interactions, Can. J. Chem. 73 (1995) 1711.
[50] B.K. Kim, S. Sy, A. Yu, J. Zhang, Electrochemical Supercapacitors for Energy Storage and Conversion, in: Handbook of Clean Energy Systems John Wiley & Sons, Ltd (2015).
[51] A. Laheaeaer, P. Przygocki, Q. Abbas, F. Beguin, Appropriate methods for evaluating the efficiency and capacitive behavior of different types of supercapacitors, Electrochem. Commun. 60 (2015) 21.
[52] B. Muthulakshmi, D. Kalpana, S. Pitchumani, N.G. Renganathan, Electrochemical deposition of polypyrrole for symmetric supercapacitors, J. Power Sources 158 (2006) 1533.
[53] L.F.Q.P. Marchesi, F.R. Simoes, L.A. Pocrifka, E.C. Pereira, Investigation of Polypyrrole Degradation Using Electrochemical Impedance Spectroscopy, J. Phys. Chem. B 115 (2011) 9570.
[54] L.F. Marchesi, S.C. Jacumasso, R.C. Quintanilha, H. Winnischofer, M. Vidotti, The electrochemical impedance spectroscopy behavior of poly(aniline) nanocomposite electrodes modified by Layer-by-Layer deposition, Electrochim. Acta 174 (2015) 864.
[55] H. Du, Y. Wang, H. Yuan, L. Jiao, Facile Synthesis and High Capacitive Performance of 3D Hierarchical Ni(OH)2 Microspheres, Electrochim. Acta 196 (2016) 84.
[56] Y. Zhao, H. Wei, M. Arowo, X. Yan, W. Wu, J. Chen, Y. Wang, Z. Guo, Electrochemical energy storage by polyaniline nanofibers: high gravity assisted oxidative polymerization vs. rapid mixing chemical oxidative polymerization, Phys. Chem. Chem. Phys. 17 (2015) 1498.
[57] T. Li, Z. Qin, B. Liang, F. Tian, J. Zhao, N. Liu, M. Zhu, Morphology-dependent capacitive properties of three nanostructured polyanilines through interfacial polymerization in various acidic media, Electrochim. Acta 177 (2015) 343.
[58] X. Wu, Q. Wang, W. Zhang, Y. Wang, W. Chen, Nano nickel oxide coated graphene/polyaniline composite film with high electrochemical performance for flexible supercapacitor, Electrochim. Acta 211 (2016) 1066.
[59] L. Hostert, G. de Alvarenga, M. Vidotti, L.F. Marchesi, Sonoelectrodeposition of poly(pyrrole) films: Electrochemical and morphological effects caused by the ultrasonic amplitude, J. Electroanal. Chem. 774 (2016) 31.
[60] L.F. Marchesi, E.C. Pereira, The influence of the drying process on electrochemical properties of P3HT/PCBM (1.00/0.25 wt%) electrodes, Synth. Met. 194 (2014) 82.